Chaos in a tunneling universe

Journal of Cosmology and Astroparticle Physics
An IOP and SISSA journal

Chaos in a tunneling universe

Martin Bojowald and Ari Gluckman

Department of Physics, The Pennsylvania State University,
104 Davey Lab, University Park, PA 16802, U.S.A.

E-mail: bojowald@psu.edu, ayg5136@psu.edu

Received July 7, 2023
Revised September 15, 2023
Accepted October 17, 2023
Published November 13, 2023

Abstract. A recent quasiclassical description of a tunneling universe model is shown to exhibit chaotic dynamics by an analysis of fractal dimensions in the plane of initial values. This result relies on non-adiabatic features of the quantum dynamics, captured by new quasiclassical methods. Chaotic dynamics in the early universe, described by such models, implies that a larger set of initial values of an expanding branch can be probed.

Keywords: quantum cosmology, initial conditions and eternal universe

ArXiv ePrint: 2307.03145

https://doi.org/10.1088/1475-7516/2023/11/052

JCAP11(2023)052

Contents

1 Introduction

Quantum effects such as tunneling may be relevant in the early universe at high temperature and curvature. Early models [1] have recently been extended to oscillating versions [2, 3] in which the evolving scale factor, classically trapped in a finite region, may escape by quantum tunneling and approach a singularity [4–6]. An application [7] of quasiclassical methods revealed non-trivial features of the tunneling dynamics that is not captured by the traditional derivation of tunneling coefficients from stationary states. In particular, some of the dynamics was found to depend sensitively on the choice of initial values in the trapped region, suggesting chaotic behavior. The purpose of the present paper is to confirm this suspicion by a dedicated analysis.

The physical relevance of chaos in universe models can be seen by going beyond the first approximation of an exactly homogeneous universe. At low curvature, observations of large-scale structure indicate that approximate spatial homogeneity is a good late-time assumption, but it is unlikely to hold in the early universe. At large density and curvature, the gravitational dynamics is rather dominated by attraction to denser regions and their subsequent collapse, suggesting a very inhomogeneous distribution out of which our universe may have arisen by cosmic inflation. The corresponding rapid expansion would then have magnified and diluted a small region that eventually formed our visible universe. In the initial distribution, however, this small region would have been only one tiny patch. Thanks to its smallness, it may be assumed to be nearly homogeneous and approximately described by simple (classical or quantized) Friedmann dynamics. But its properties were determined by high-density features that are more involved than those tested at late times.

It has been known for some time that the classical dynamics of such a patch is chaotic [8–11], provided it includes effects of anisotropy (while still being spatially homogeneous). Such a dynamics is expected asymptotically close to a spacelike singularity according to the Belinskii-Khalatnikov-Lifshitz (BKL) scenario [12]. Given the asymptotic nature of this model, the effects of this kind of chaos are most pronounced in backward evolution closer and closer to the big-bang singularity. They are therefore relevant for a conceptual analysis of possible initial conditions at the very beginning of the universe, but their implications for potential observations, seen for instance through the magnifying glass of inflation, would be rather indirect.

Once certain matter effects start being relevant, the anisotropic asymptotic geometry may isotropize [13], a property that is also desirable for models of inflation. In an intermediate

JCAP11(2023)052

phase between an asymptotically early BKL regime and the (still early) beginning of inflation, anisotropy may be ignored while quantum effects are strong. The results presented here show that even the isotropic dynamics is chaotic if it is described quasiclassically by including quantum fluctuation terms, applied in the specific analysis to tunneling-type potentials as in oscillating models. We will use the same model and quasiclassical extensions as derived in [7], reviewed in the next section, and show proofs of chaos based on a numerical analysis of the fractal domension in a space of initial values. In our conclusions we will demonstrate which features of the specific potential are likely to be responsible for chaos. Compared with BKL-type chaos, the new chaotic features identified here, closer to the onset of inflation, may have phenomenological implications which we leave for future analysis.

2 Quasiclassical model

The classical model and its potential, introduced in [3] follow from the Friedmann equation

$$\frac{\dot{a}^2}{a^2} + \frac{k}{a^2} = \frac{8\pi G}{3}\left(\Lambda + \frac{\sigma}{a} + \frac{p_\phi^2}{2a^6}\right) \tag{2.1}$$

with positive spatial curvature, $k > 0$, a negative cosmological constant $\Lambda < 0$, and two matter contributions, one with energy density σ/a where $\sigma > 0$, and one from a free, massless scalar field ϕ with momentum p_ϕ. Our results do not depend much on the specific features of the contributions from σ and p_ϕ, other than the trapped potential region they form together with the curvature term. For the latter, we choose $k = 1$, but smaller values are also possible; see [7, 14] for more details.

The quasiclassical methods we use are canonical. We therefore replace the time derivative $\dot{a}$ of the scale factor with the standard momentum

$$p_a = -\frac{3}{4\pi G} a\dot{a} \tag{2.2}$$

in Friedmann cosmology; see for instance [15]. The Friedmann equation (2.1) can then be written as

$$0 = \frac{16}{9}\pi^2 G^2 p_a^2 + a^2 U_{\rm harmonic}(a) - \frac{\tilde{p}^2}{a^2} \tag{2.3}$$

with a harmonic potential

$$U_{\rm harmonic}(a) = \omega^2(a - \gamma/\omega)^2 + k - \gamma^2 \tag{2.4}$$

expressed in terms of the parameters

$$\omega = \sqrt{-\frac{8\pi G\Lambda}{3}} \quad \text{and} \quad \gamma = \sqrt{-\frac{2\pi G\sigma^2}{3\Lambda}}\,. \tag{2.5}$$

The scalar contribution is not harmonic, and only slightly rewritten by introducing

$$\tilde{p} = \sqrt{\frac{4\pi G}{3}} p_\phi\,. \tag{2.6}$$

Finally, we perform a canonical transformation from (a, p_a) to (α, p_α) where

$$\alpha = \ln(\omega\gamma a) \tag{2.7}$$

JCAP11(2023)052

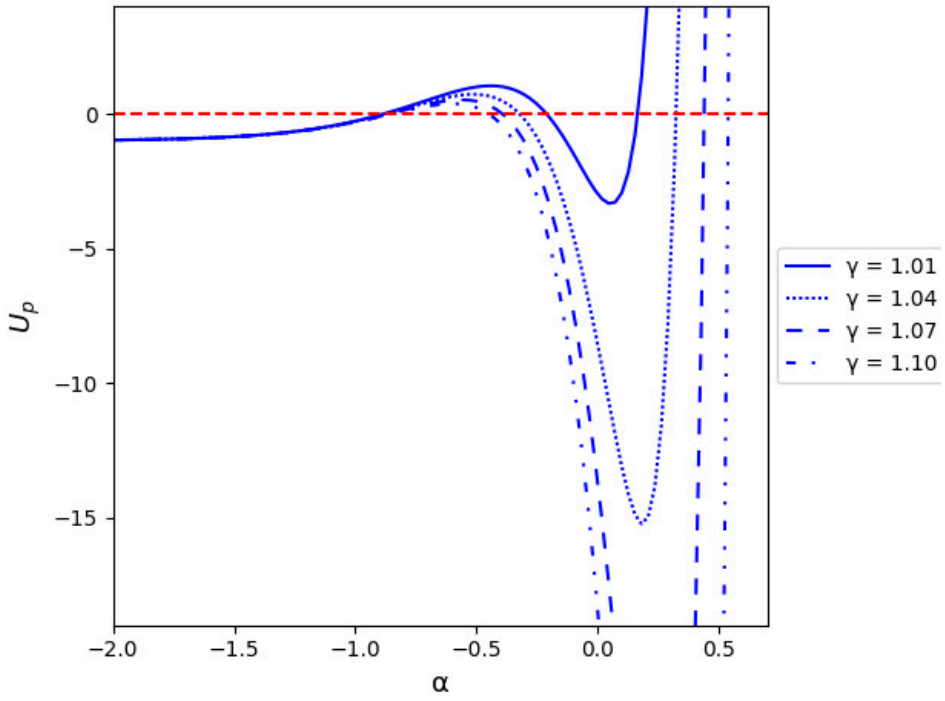

Figure 1. The potential (2.10) for several values of γ, with fixed $\beta = 0.1$ and $p = 1$ as well as $k = 1$.

and

$$p_\alpha = a p_a = -\frac{3}{4\pi G} a^2 \dot{a} \,. \tag{2.8}$$

In these variables, the Friedmann equation is equivalent to

$$0 = p_\alpha^2 + U_p(\alpha) \tag{2.9}$$

with the potential

$$U_p(\alpha) = \frac{e^{4\alpha}}{\beta^2}\left(k - 2e^\alpha + \frac{e^{2\alpha}}{\gamma^2}\right) - p^2 \tag{2.10}$$

and

$$\beta = \frac{4\pi G}{3}\omega^2\gamma^2 = \left(\frac{4\pi G}{3}\right)^3 \sigma^2 \,, \qquad p = \frac{3}{4\pi G}\tilde{p} = \sqrt{\frac{3}{4\pi G}} p_\phi \,. \tag{2.11}$$

As shown in figure 1, the contribution from the scalar field can now be seen as opening up a classically allowed region around $\alpha \to -\infty$, making it possible for the universe to tunnel from the trapped region, formed by the other contributions, to a big-bang singularity. On the other side of the α-axis, expansion to infinite size is prevented by the steep positive potential contribution proportional to $e^{6\alpha}$, which is implied by the negative cosmological constant. The density contribution σ/a provides a negative contribution to the potential $U_p(\alpha)$ that forms a trapped region at intermediate values of α, separated from the asymptotic free region around $\alpha \to -\infty$ by a positive barrier implied by the curvature term. For the intermediate negative contribution to form a trapped region, it must be dominant between the two regions implied by the contributions from spatial curvature and the cosmological constant, respectively. In the original Friedmann equation, the corresponding energy density must therefore follow a behavior between the power laws a^{-2} of the curvature term and a^0 of

JCAP11(2023)052

the cosmological constant. This requirement explains the non-standard a-dependence of the energy density σ/a.

The quasiclassical dynamics of a given classical system in canonical form is obtained by viewing variables such as α and p_α as expectation values of the corresponding operators, taken in an evolving quantum state. Any non-harmonic potential then implies that these variables couple to fluctuations, correlations, and higher moments, implying dynamics in a higher-dimensional configuration space. Coupling terms can be derived by equipping moments with a Poisson bracket and inserting them in the expectation value of the Hamilton operator of the system, taken in the same state in which the moments are computed [16, 17]. In general, the usual central moments do not immediately appear in canonically conjugate form, but suitable canonical pairs exist locally thanks to the Darboux theorem. Such canonical variables have been derived for moments up to fourth order [18, 19].

For second-order moments, as a first approximation, canonical moment variables for a single pair of degrees of freedom, such as (α, p_α) here, have been known for some time, discovered independently in a variety of fields [20–25]: There is an independent canonical pair (s, p_s) that describes second-order moments according to

$$\Delta(\alpha^2) = s^2 \tag{2.12}$$

$$\Delta(\alpha p_\alpha) = s p_s \tag{2.13}$$

$$\Delta(p_\alpha^2) = p_s^2 + \frac{U}{s^2}\,, \tag{2.14}$$

where U is a constant bounded from below by $U \geq \hbar^2/4$ by the uncertainty relation. We are using a general notation for moments

$$\Delta(A^a B^b) = \left\langle (\hat{A} - \langle \hat{A}\rangle)^a (\hat{B} - \langle \hat{B}\rangle)^b \right\rangle_{\rm symm} \tag{2.15}$$

in completely symmetric (or Weyl) ordering. According to this notation, the two variances for a single canonical pair are $(\Delta\alpha)^2 = \Delta(\alpha^2)$ and $(\Delta p_\alpha)^2 = \Delta(p_\alpha^2)$ and the covariance is $\Delta(\alpha p_\alpha)$.

If the classical Hamiltonian is $H(\alpha, p_\alpha)$, the new canonical variables for second-order moments can be introduced in an effective Hamiltonian by performing a Taylor expansion of $H(\alpha + \delta\alpha, p_\alpha + \delta p_\alpha)$ around a generic pair (α, p_α) and replacing terms quadratic in $\delta\alpha$ and δp_α with the moments (2.12)–(2.14). The effective energy expression, derived from (2.9) in the cosmological model, then reads

$$0 = p_\alpha^2 + p_s^2 + \frac{U}{s^2} + U_p(\alpha) + \frac{1}{2} U_p''(\alpha) s^2 \tag{2.16}$$

where $U_p(\alpha)$ is given in (2.10). (The classical equation (2.9) is a Hamiltonian constraint, which in a quantization is turned into a constraint operator that annihilates physical states. This condition restricts not only expectation values of basic operators by an equation approximated by (2.16) semiclassically, but also fluctuations and higher moments of the state [26–28]. Since the constraint does not depend on ϕ but only on its momentum, we can assume that moment constraints are solved by using restricted values for ϕ-moments. The latter do not appear in the effective constraint and we do not need specific solutions for them.)

While the momentum dependence of (2.9) is quadratic and does not imply higher-order terms in the Taylor expansion, the potential is not harmonic. We therefore ignore certain quantum corrections in a truncation to second order in s, given by (2.16). Tunneling, a process during which a wave packet splits up into at least two smaller packets, is likely to

JCAP11(2023)052

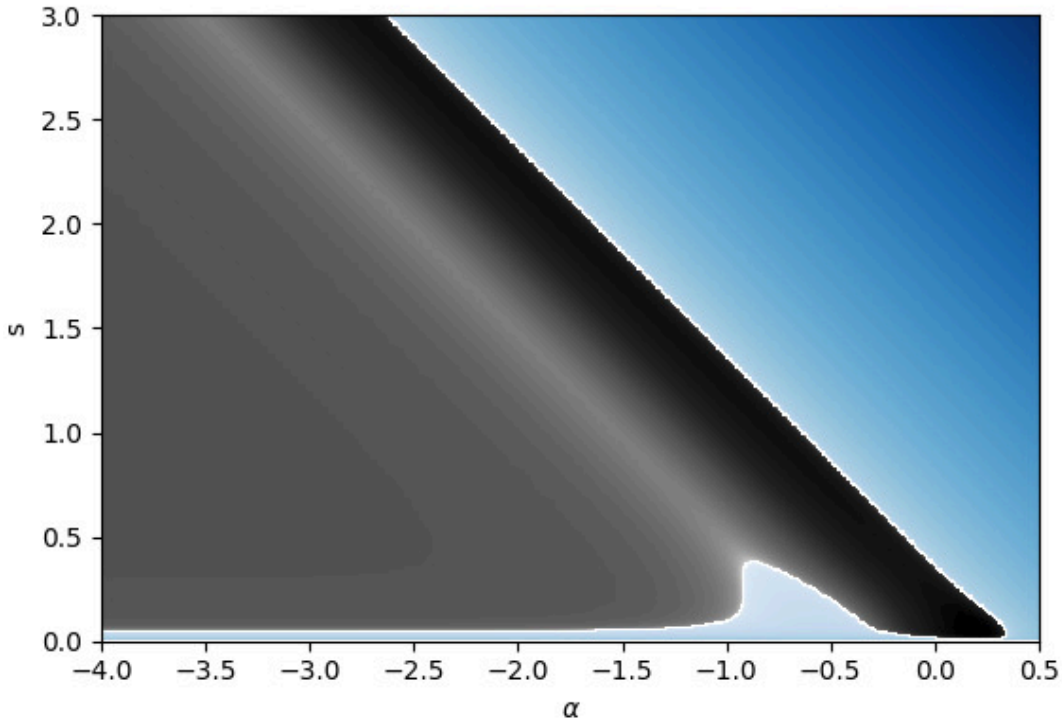

Figure 2. Contour plot of the quasiclassical potential in (2.17). Negative values of the potential are shown in shades of gray, while positive values are in blue. The black region crossing the figure in a diagonal way is the deep channel that extends the trapped region into the s-dimension. The thinner light-gray strip that bounds the channel on its left flank is an elevation in the region of negative potential implied by the classical barrier. For a complete description of tunneling, trajectories in the quasiclassical model must cross the elevation once in the past and in the future of being trapped.

depend on moments of order higher than two. We should therefore amend (2.16) by suitable higher-order terms, while keeping the system sufficiently simple for an initial analysis. In particular, higher-order moments, in a canonical formulation, describe degrees of freedom independent of both (α, p_α) and (s, p_s), and therefore lead to configuration spaces of large dimensions if they are included in complete form.

As an approximation, it is possible to include some higher-moment effects without higher dimensions by making an ansatz for the possible behavior of moments on the quantum degree of freedom (s, p_s) already introduced for second order. Dimensional arguments suggest the power-law form $\Delta(\alpha^n) \propto s^n$ for an α-moment of order n. If this form were realized exactly with coefficient one, the Taylor expansion of the effective potential could be summed up analytically:

$$0 = p_\alpha^2 + p_s^2 + \frac{U}{s^2} + U_p(\alpha) + \sum_{n=2}^{\infty} \frac{U_p^{(n)}}{n!} \Delta(\alpha^n) = p_\alpha^2 + p_s^2 + \frac{U}{s^2} + \frac{1}{2}\left(U_p(\alpha+s) + U_p(\alpha-s)\right) . \quad (2.17)$$

As in [7], following [29, 30], we bring the fourth-order term closer to Gaussian form, where $\Delta(\alpha^4) = 3s^4$ rather than s^4, by adding the final term in

$$0 = p_\alpha^2 + p_s^2 + \frac{U}{s^2} + \frac{1}{2}\left(U_p(\alpha+s) + U_p(\alpha-s)\right) + \frac{1}{12} U_p''''(\alpha) s^4 . \quad (2.18)$$

JCAP11(2023)052

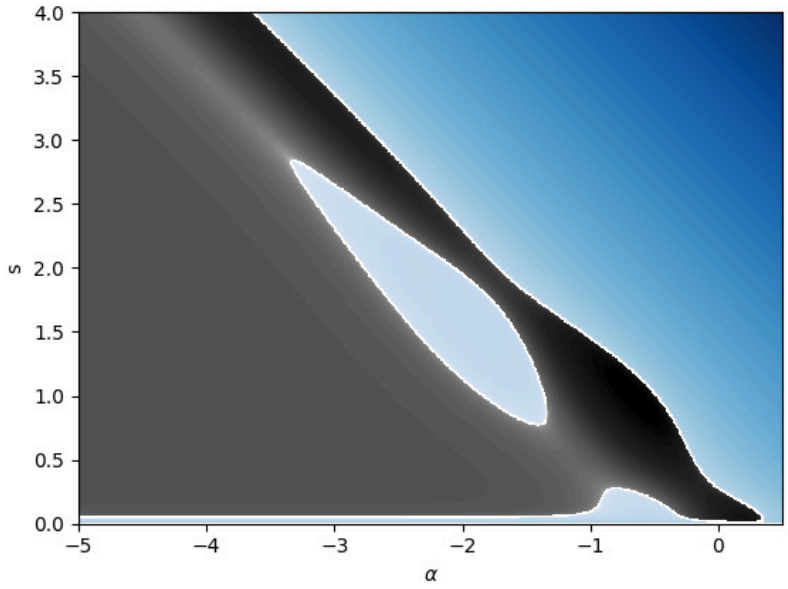

Figure 3. Contour plot of the modified quasiclassical potential (2.18) with new features in the small-s part of the channel. While keeping a door open to exit the channel at small s, the channel itself narrows such that it is less likely for quasiclassical trajectories to follow it to large s. At the same time, the new features introduce additional convex or defocusing contributions to the channel walls at small s, which are expected to enhance chaos.

Our analysis of chaos will use mainly the small-s dynamics in the trapped region before much tunneling happens, in which case the quasiclassical approximation is expected to be reliable.

3 Tunneling and chaos

Tunneling is quasiclassically described by motion in the (α, s)-plane, relying on several characteristic features of the effective potential in (2.18); see figures 2 and 3. By the addition and subtraction of s in the terms resulting from (2.17), the classically trapped region is extended to a diagonal channel in the s-direction. The channel is bounded by a finite wall to the left and a steep increasing wall to the right. Since the wall on the left has a height lower than the classical barrier for sufficiently large s, tunneling is possible when a quasiclassical trajectory crosses over the wall into the unbounded region to the left, where it will then continue almost freely except for one possible reflection at the U/s^2 potential.

A detailed analysis of trajectories, given in [7], showed that the potential (2.17) does not reliably describe tunneling because the uniform nature of the channel, seen in figure 2, makes it much more likely for trajectories to follow the channel, rather than crossing the wall to the left. The fourth-order modification in (2.18), motivated by a more Gaussian behavior of states, was found to improve the tunneling description by quasiclassical trajectories. With this modification, the channel acquires new features at small s, shown in figure 3, that can help to turn trajectories toward the channel wall. Figure 4 shows an example of a trajectory in the potential (2.18) with tunnel exits to the past and the future, indicated by differently colored branches in the figure. Each of the two parts of the trajectory outside of the channel clearly shows a reflection at the U/s^2-potential, and nearly-linear behavior away from the relfection points. The trajectory within the channel has a region where it is able to cross over

JCAP11(2023)052

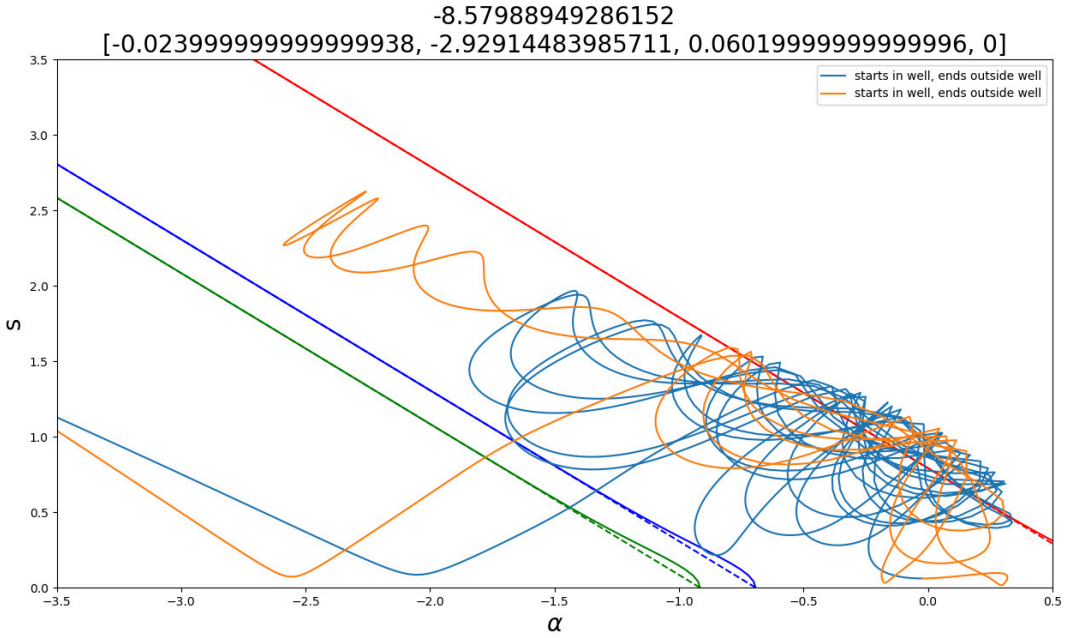

Figure 4. Example of a trajectory that tunnels in the past and in the future. The number in the top line indicates the initial potential, while initial phase-space values are given in the second line in the form $[\alpha, p_\alpha, s, p_s]$. The nearly straight dark green, blue and red lines show features of the potential walls delineating the channel, as derived in [7].

the red line on the right which marks the rightmost wall of the original potential (2.17). As seen in figure 3, the modification in the potential (2.18) dents the channel wall, allowing the trajectory to move further to the right.

However, since the quasiclassical model does not capture all features of tunneling, there are also trajectories that never cross over the wall even if their energy would be sufficient for full quantum mechanical tunneling; see figure 5. Such trajectories are stuck in the channel and keep bouncing between the two walls, moving to ever larger s. Here, the quasiclassical approximation will eventually break down.

Trajectories stuck in the channel therefore do not describe correct features of tunneling, but their presence allows us to draw an important distinction between two types of trajectories: Those that tunnel correctly by moving over the wall on the left, and those that get stuck in the channel. The latter can be split into subcases of trajectories getting stuck only to one side in time (future or past; see figure 6) or to both sides as in figure 5. Physically, any trajectory that gets stuck corresponds to a wave function for which higher moments are relevant, while trajectories that do not get stuck have a tunneling process well described by lower moments.

There were two indications for chaos in this dynamics found in [7]: A sensitive dependence of long-term outcomes of trajectories on their initial values in the classically trapped region; and the shape of the confining walls around the classically trapped region, extended to the (α, s)-plane. Since the latter have convex or defocussing contributions, especially with the fourth-order modification as seen in figure 3, mathematical arguments from dynamical billiard systems may be used to infer the possibility of chaotic features [31], as done also in other cosmological models [11]. However, the walls are not completely convex. A dedicated analysis is therefore required to determine properties of chaos [32]. We do so now by numerical

JCAP11(2023)052

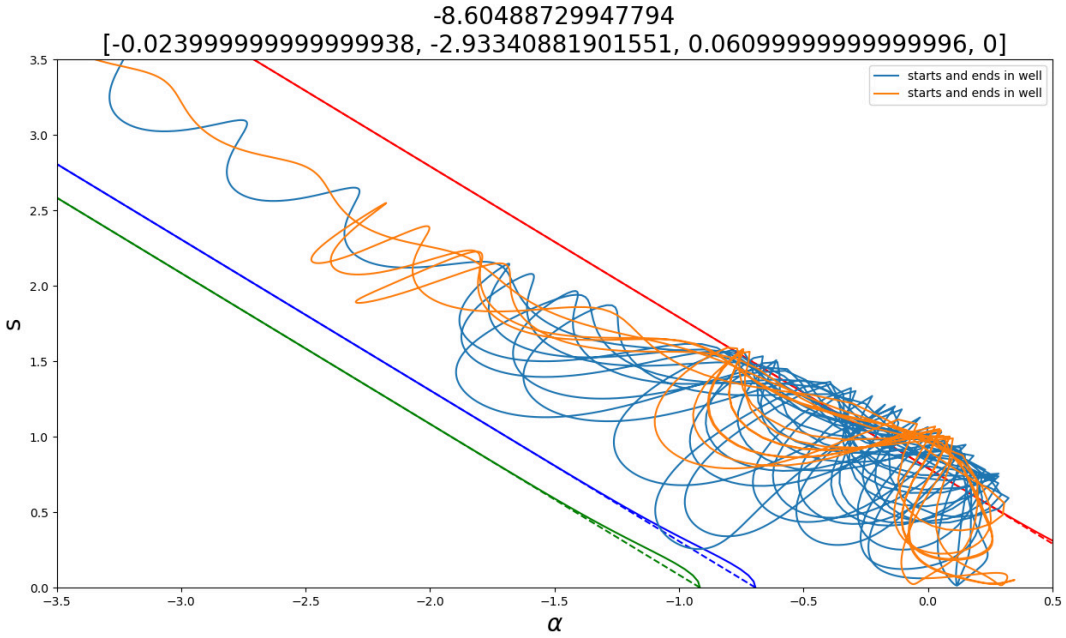

Figure 5. Example of a trajectory that never tunnels. The number in the top line indicates the initial potential, while initial phase-space values are given in the second line in the form $[\alpha, p_\alpha, s, p_s]$.

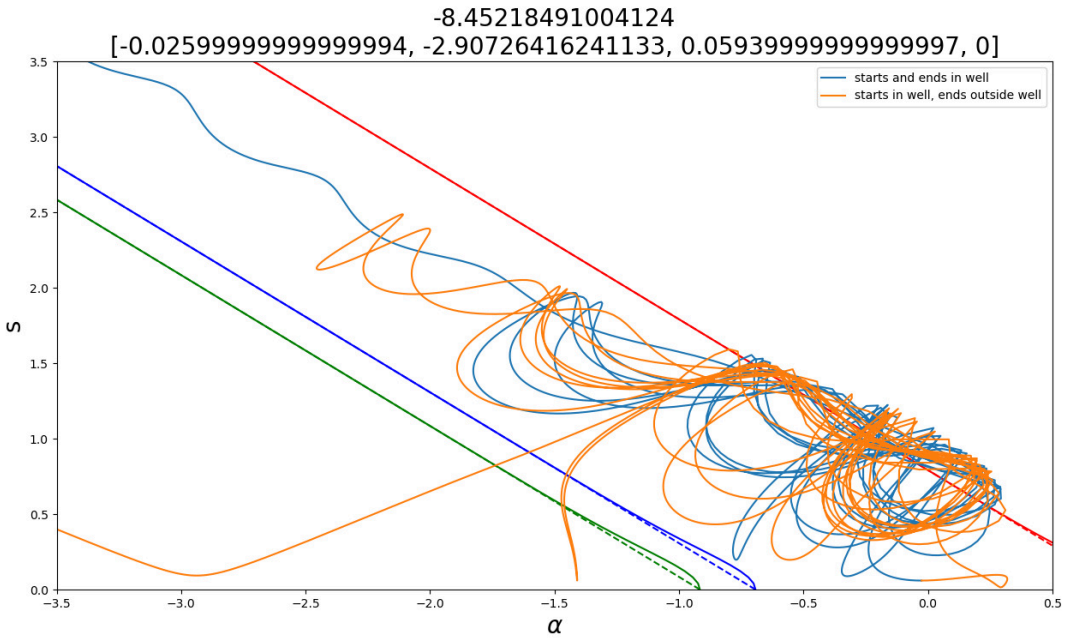

Figure 6. Example of a trajectory that tunnels only once in the past or future. The number in the top line indicates the initial potential, while initial phase-space values are given in the second line in the form $[\alpha, p_\alpha, s, p_s]$.

JCAP11(2023)052

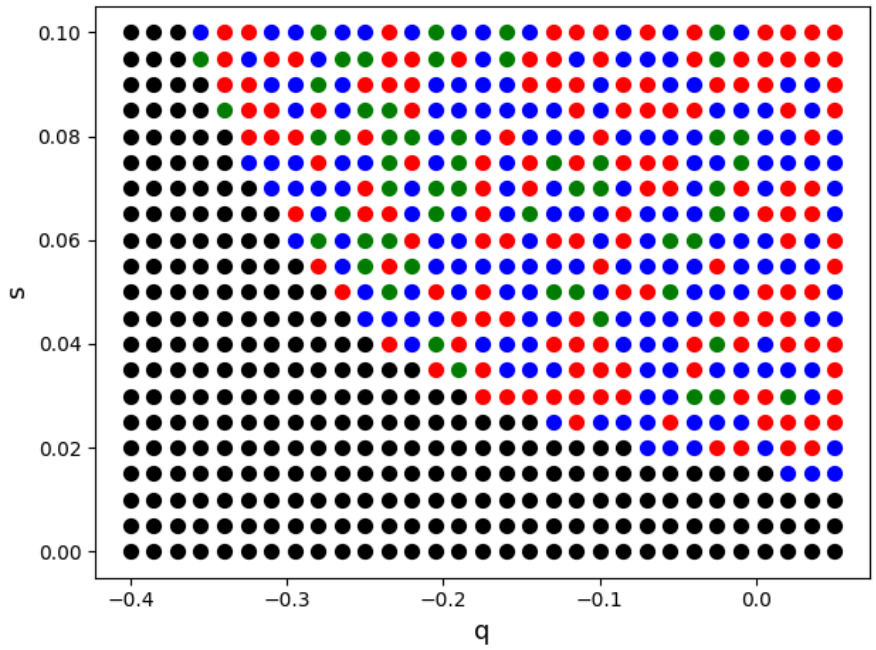

Figure 7. An initial 20×20 lattice of outcomes, depending on the initial values of $q = \alpha$ and s. Within this lattice, initial points are marked with colors depending on the long-term outcome of trajectories starting there, all with the same initial momenta $p_\alpha = 0.075$ and $p_s = 0$. The red points indicate initial conditions that never tunnel (as in figure 5), blue points indicate initial conditions that tunnel once (in the future or past, as in figure 6), and green points indicate initial conditions that tunnel in and out (as in figure 4). The black region is outside the channel walls and does not lead to tunneling.

computations of the fractal dimension of sets of initial values in the bottom part of the channel that give rise to the same long-term outcome of tunneling trajectories. The sensitivity to the choice of initial values is illustrated by figures 7 and 8.

The procedure for calculating the fractal dimension of the model and demonstrating chaos involved generating a 50×50 lattice of distinct tunneling results, illustrated in figure 8. (The lattice size is limited by computational time since each lattice point requires a long-term numerical evolution with sufficient accuracy to resolve many oscillations and sharp turns as seen in figures 4–6.) Based on the numerically evolved trajectories, which were obtained using standard built-in methods in Python, the lattice points in the sample region were classified as fully trapped, partially trapped, or untrapped. These outcomes therefore define subregions on the lattice with boundaries whose fractal dimension may present an indicator of chaos.

The lattice was analyzed by using the basin method [33] which looks for fractal dimensions in boundaries of different subregions, defined here by the different outcomes of our trajectories. Here, the subregions are defined on the lattice. Intuitively, if we look at small regions around each lattice point, there will be few variations in the outcomes if subregions have non-fractal boundaries, and larger variations if the boundaries have fractal dimensions. The numerical evaluation therefore begins with a fixed small value δ that defines the radius of a small circle around each lattice point (or, more generally, some size measure of a different shape). For each lattice point, the number of points within a distance of δ with outcomes different from the central point is then counted. The fraction of points with different outcomes relative to

JCAP11(2023)052

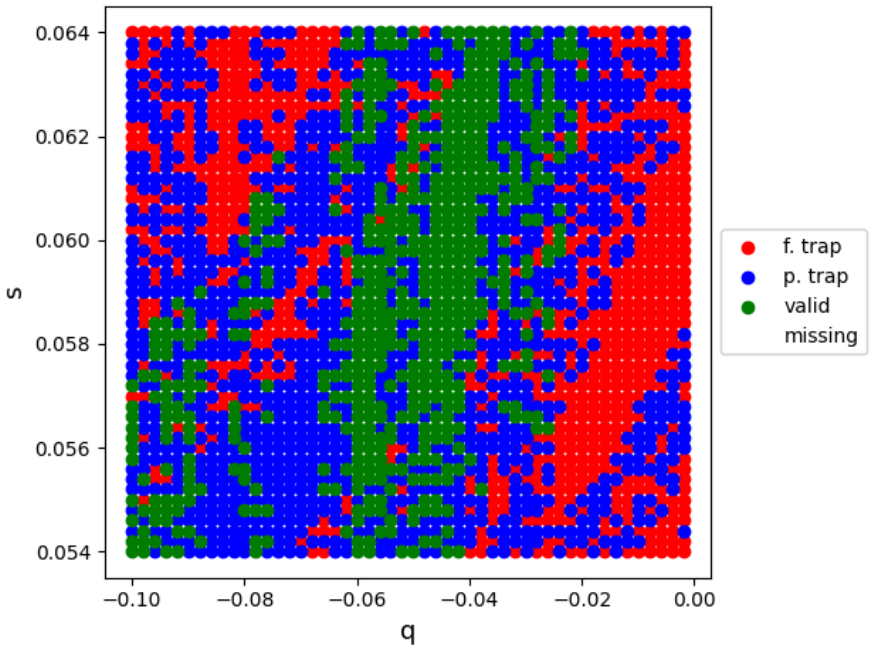

Figure 8. A finer sublattice of figure 7 with 50×50 lattice points, revealing new structures of independent outcomes, using the same color code. The region used here is completely contained in the channel.

the number of all lattice points within the small δ-region is the basic quantity computed by the method. Averaged over all lattice points as centers of δ-regions, it defines the value $f(\delta)$, first for a given δ. The procedure is then repeated for other values, yielding several points on the graph of a function $f(\delta)$.

For non-fractal boundaries of codimension C, the function $f(\delta)$ is expected to be a power law $f(\delta) \propto \delta^C$ because increasing δ makes it more likely to include a new boundary in a circle of radius δ if the circle extends further in directions transversal to the nearest boundary. In our case, the codimension is one, and therefore $f(\delta) \propto \delta$ for non-fractal boundaries. Since $C = D - D_0$ where D is the dimension of the space and D_0 the dimension of the boundary, we have

$$f(\delta) \propto \delta^{D-D_0} \,. \tag{3.1}$$

This expression can directly be generalized to fractal boundaries where D_0 is not an integer, such that we have

$$f(\delta) \sim \delta^{\epsilon} \tag{3.2}$$

with the so-called uncertainty exponent ϵ. In general, ϵ may depend on δ, but a power-law form may be used as a first approximation. Numerically, ϵ can be determined from a fit of the values $f(\delta)$, which then defines the fractal dimension

$$D_0 = D - \epsilon \tag{3.3}$$

of the boundaries.

The range of ϵ for chaotic systems is given by $0 \leq \epsilon < 1$. Lower values of ϵ indicate that the boundaries are denser in the lattice, making it more likely for small changes of the

JCAP11(2023)052

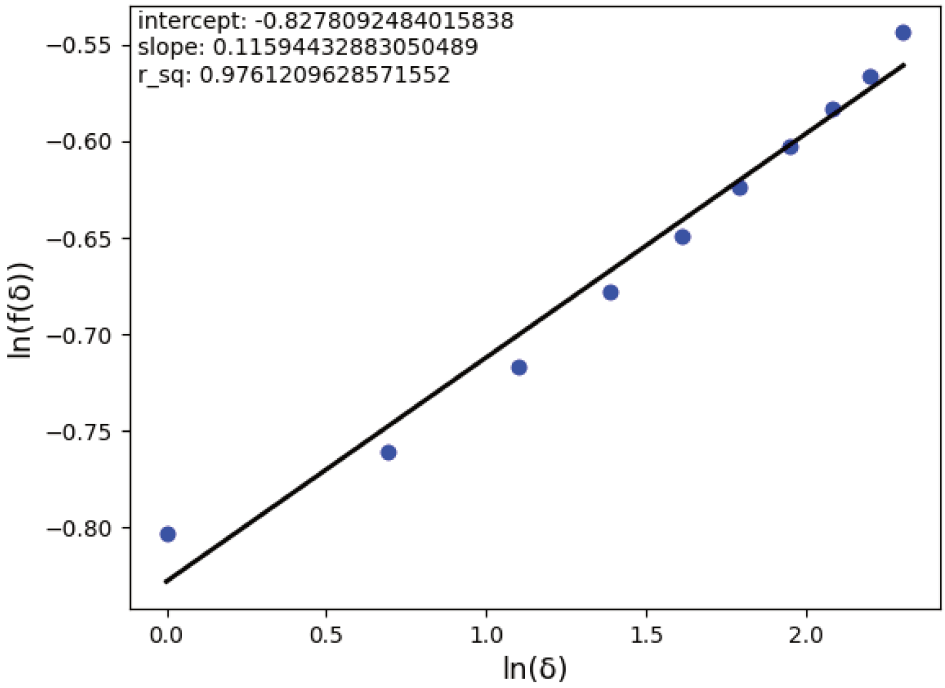

Figure 9. Linear fit to a double-logarithmic plot of (3.2), where δ is measured in integer multiples of the lattice spacing shown in figure 8. The slope of the fit is our result for ϵ. At a value of about 0.116, it is significantly less than one and strongly indicates chaos. The quality of the statistical fit is high, as shown by an R^2-value very close to one.

initial point to imply significant changes of the outcome. The system is then more chaotic. As emphasized in [9], measuring chaos using this basin method [33] is more suitable for relativistic or time reparameterization invariant systems because it depends only on the final outcomes of trajectories and not on their parameterization by time, unlike for instance the computation of Lyapunov exponents. Reparameterization of the time variable will not alter the final states indicated on the lattice. As also used recently in [34], the method can easily be generalized to quasiclassical descriptions of quantum systems.

Computing the value of ϵ for the model, following the numerical procedure outlined in appendix A, produced figure 9, using values $1 \leq \delta \leq 10$. A linear fit of the data in a double logarithmic plot revealed the slope $\epsilon = 0.116$ or a fractal dimension of $D_0 = 1.884$ for the boundaries, and is thus a strong indicator of chaos. The large R^2-value of the fit, given by 0.976, shows that the power-low (3.2) is a good approximation in this case, even though ϵ may not be strictly constant.

4 Conclusions

Our results demonstrate that the quasiclassical dynamics of the oscillating universe model studied here is chaotic. The classical system has a 1-dimensional configuration space and therefore cannot have chaos, but quantization implies additional independent degrees of freedom such as the fluctuation parameter s in our analysis. The appearance of chaos here is therefore distinct from the traditional notion of quantum chaos, which is usually analyzed in situations in which the classical system is already chaotic.

JCAP11(2023)052

Our model is closer to discussions of chaos in Bohmian quantum mechanics, such as [35–37], in which the quantum potential plays the role of our quasiclassical potential. Compared with Bohmian quantum mechanics, our analysis is held completely at a phase-space level as in classical mechanics. Quantum effects are described by moments in a canonical parameterization, implying new configuration variables and momenta. The full wave function is approximated and ultimately replaced by the moments and does not play an intermediary role, for instance as the wave function of Bohmian quantum mechanics used to compute the quantum potential. Standard quantitative methods to analyze chaos can therefore be applied directly.

A qualitative argument, using the convex nature of some portions of the potential walls bounding the quasiclassical trapped region, demonstrate a relationship between chaos and detailed properties of the quantum state. In particular, our quantitative results about chaos refer to a quasiclassical potential with fourth-order moments of Gaussian form, which compared with other choices of moments leads to more convex walls as seen in figure 3. Our results therefore suggest that details of quantum states and properties of their quantum information may have direct implications on important features of the early-universe dynamics.

Acknowledgments

We are grateful to Sara Fernández Uria for bringing our attention to the basin method and for discussions about it. This work was supported in part by NSF grant PHY-2206591.

A Description of the numerical code

Our code that computes the fractal dimension consists of different parts, some of which use standard methods. These parts include numerical evolution to find trajectories and their long-term outcomes starting with various initial values on a lattice, and organizing these outcomes in a suitable data structure. Once the outcomes are assembled in an array that reproduces our lattice, the following calculations are performed in separate procedures:

Computation of an uncertainty ratio for a given δ at fixed lattice point. For the sake of simplicity, we used diamond-shaped regions instead of circles. Two for-loops over integer ranges from $-\delta$ to δ first define a square region, which is then restricted to a diamond by imposing the condition $|\Delta x| + |\Delta y| \leq \delta$ on the displacements Δx and Δy. For each non-zero $|\Delta x| + |\Delta y|$, a counter is increased if the outcome at the displaced point is different from the outcome of the central point. The result of this computation is the ratio of the counter divided by the number of points in the region.

Computation of $f(\delta)$ for a given δ. The uncertainty ratios obtained in the previous step are averaged over the entire lattice, resulting in the value of $f(\delta)$ for a given δ. This computation is performed for a range of δ, in our case integers from one to ten.

Computation of the uncertainty exponent and related data. Linear regression is applied to the result $f(\delta)$ of the previous step. The slope is the numerical value for the uncertainty exponent ϵ. The intercept is not of interest in this case, but standard procedures also provide an estimate of R^2 that can be used to judge the reliability of the fit. In the present case, larger values of R^2 correspond to more constant $\epsilon(\delta)$.

JCAP11(2023)052

References

[1] A. Vilenkin, *Quantum Creation of Universes*, *Phys. Rev. D* **30** (1984) 509 [INSPIRE].

[2] M.P. Dąbrowski, *Oscillating Friedman cosmology*, *Annals Phys.* **248** (1996) 199 [gr-qc/9503017] [INSPIRE].

[3] P.W. Graham et al., *A Simple Harmonic Universe*, *JHEP* **02** (2014) 029 [arXiv:1109.0282] [INSPIRE].

[4] M.P. Dąbrowski and A.L. Larsen, *Quantum tunneling effect in oscillating Friedmann cosmology*, *Phys. Rev. D* **52** (1995) 3424 [gr-qc/9504025] [INSPIRE].

[5] A.T. Mithani and A. Vilenkin, *Collapse of simple harmonic universe*, *JCAP* **01** (2012) 028 [arXiv:1110.4096] [INSPIRE].

[6] A.T. Mithani and A. Vilenkin, *Tunneling decay rate in quantum cosmology*, *Phys. Rev. D* **91** (2015) 123511 [arXiv:1503.00400] [INSPIRE].

[7] M. Bojowald and P. Petersen, *Tunneling dynamics of an oscillating universe model*, *JCAP* **05** (2022) 007 [arXiv:2110.09491] [INSPIRE].

[8] J.D. Barrow, *Chaotic behavior in general relativity*, *Phys. Rept.* **85** (1982) 1 [INSPIRE].

[9] N.J. Cornish and J.J. Levin, *The mixmaster universe: A Chaotic Farey tale*, *Phys. Rev. D* **55** (1997) 7489 [gr-qc/9612066] [INSPIRE].

[10] A.E. Motter, *Relativistic chaos is coordinate invariant*, *Phys. Rev. Lett.* **91** (2003) 231101 [gr-qc/0305020] [INSPIRE].

[11] T. Damour, M. Henneaux and H. Nicolai, *Cosmological billiards*, *Class. Quant. Grav.* **20** (2003) R145 [hep-th/0212256] [INSPIRE].

[12] V. Belinsky, I. Khalatnikov and E. Lifshitz, *A General Solution of the Einstein Equations with a Time Singularity*, *Adv. Phys.* **31** (1982) 639 [INSPIRE].

[13] C.W. Misner, *The isotropy of the universe*, *Astrophys. J.* **151** (1968) 431 [INSPIRE].

[14] M. Bojowald, *The BKL scenario, infrared renormalization, and quantum cosmology*, *JCAP* **01** (2019) 026 [arXiv:1810.00238] [INSPIRE].

[15] M. Bojowald, *Foundations of Quantum Cosmology*, IOP (2020) [DOI:10.1088/2514-3433/ab9c98] [INSPIRE].

[16] M. Bojowald and A. Skirzewski, *Effective equations of motion for quantum systems*, *Rev. Math. Phys.* **18** (2006) 713 [math-ph/0511043] [INSPIRE].

[17] M. Bojowald and A. Skirzewski, *Quantum gravity and higher curvature actions*, *Int. J. Geom. Meth. Mod. Phys.* **4** (2007) 25 [*eConf* **C0602061** (2006) 03] [hep-th/0606232] [INSPIRE].

[18] B. Baytaş, M. Bojowald and S. Crowe, *Faithful realizations of semiclassical truncations*, *Annals Phys.* **420** (2020) 168247 [arXiv:1810.12127] [INSPIRE].

[19] B. Baytaş, M. Bojowald and S. Crowe, *Effective potentials from semiclassical truncations*, *Phys. Rev. A* **99** (2019) 042114 [arXiv:1811.00505] [INSPIRE].

[20] R. Jackiw and A. Kerman, *Time Dependent Variational Principle and the Effective Action*, *Phys. Lett. A* **71** (1979) 158 [INSPIRE].

[21] F. Arickx, J. Broeckhove, W. Coene and P.V. Leuven, *Gaussian wave-packet dynamics*, *Int. J. Quant. Chem.* **30** (1986) 471.

[22] R.A. Jalabert and H.M. Pastawski, *Environment-Independent Decoherence Rate in Classically Chaotic Systems*, *Phys. Rev. Lett.* **86** (2001) 2490 [cond-mat/0010094].

[23] O.V. Prezhdo, *Quantized hamilton dynamics*, *Theor. Chem. Acc.* **116** (2005) 206.

JCAP11(2023)052

[24] T. Vachaspati and G. Zahariade, *Classical-quantum correspondence and backreaction*, *Phys. Rev. D* **98** (2018) 065002 [arXiv:1806.05196] [INSPIRE].

[25] M. Mukhopadhyay and T. Vachaspati, *Rolling classical scalar field in a linear potential coupled to a quantum field*, *Phys. Rev. D* **100** (2019) 096018 [arXiv:1907.03762] [INSPIRE].

[26] M. Bojowald, B. Sandhöfer, A. Skirzewski and A. Tsobanjan, *Effective Constraints for Quantum Systems*, *Rev. Math. Phys.* **21** (2009) 111 [arXiv:0804.3365] [INSPIRE].

[27] M. Bojowald and A. Tsobanjan, *Effective Constraints for Relativistic Quantum Systems*, *Phys. Rev. D* **80** (2009) 125008 [arXiv:0906.1772] [INSPIRE].

[28] M. Bojowald and A. Tsobanjan, *Effective Constraints and Physical Coherent States in Quantum Cosmology: A Numerical Comparison*, *Class. Quant. Grav.* **27** (2010) 145004 [arXiv:0911.4950] [INSPIRE].

[29] M. Bojowald et al., *Quantum Higgs Inflation*, *Phys. Lett. B* **816** (2021) 136193 [arXiv:2011.02355] [INSPIRE].

[30] M. Bojowald et al., *Multi-field inflation from single-field models*, *JCAP* **08** (2021) 047 [arXiv:2011.02843] [INSPIRE].

[31] Y.G. Sinai, *Dynamical systems with elastic reflections*, *Russ. Math. Surv.* **25** (1970) 137.

[32] L.A. Bunimovič, *On Billiards Close to Dispersing*, *Sbornik: Mathematics* **23** (1974) 45.

[33] S.W. McDonald, C. Grebogi, E. Ott and J.A. Yorke, *Fractal basin boundaries*, *Physica D* **17** (1985) 125.

[34] M. Bojowald, D. Brizuela, P.C. Cabrera and S.F. Uria, *The chaotic behavior of the Bianchi IX model under the influence of quantum effects*, arXiv:2307.00063 [INSPIRE].

[35] A.C. Tzemos, G. Contopoulos and C. Efthymiopoulos, *Origin of chaos in 3-d Bohmian trajectories*, arXiv:1609.07069 [DOI:10.1016/j.physleta.2016.09.016].

[36] G. Contopoulos and A.C. Tzemos, *Chaos in Bohmian Quantum Mechanics: A short review*, arXiv:2009.05867 [DOI:10.1134/S1560354720050056].

[37] A.C. Tzemos and G. Contopoulos, *Bohmian quantum potential and chaos*, *Chaos Solitons Fractals* **160** (2022) 112151.

JCAP11(2023)052